Non-covalently crosslinked chitosan nanofibrous mats prepared by electrospinning as substrates for soft tissue regeneration

Non-covalently crosslinked chitosan nanofibrous mats prepared by electrospinning as substrates for soft tissue regeneration

Chiara Tonda-Turo[1], Francesca Ruini[1], Martina Ramella[2], Francesca Boccafoschi[2], Piergiorgio Gentile[3], Emilia Gioffredi[1], Giuseppe Falvo D'Urso Labate [4], Gianluca Ciardelli[1]

[1]Department of Mechanical and Aerospace Engineering, Politecnico di Torino, Corso Duca degli Abruzzi 24, 10129 Torino, Italy

francesca.ruini@polito.it, emilia.gioffredi@polito.it, gianluca.ciardelli@polito.it

[2] Department of Health Sciences, University of Piemonte Orientale Novara, Via Solaroli 17, 28100 Novara, Italy

martina.ramella@med.uniupo.it, francesca.boccafoschi@med.uniupo.it

[3] School of Mechanical and Systems Engineering, Newcastle University, Claremont Road, Newcastle upon Tyne, NE1 7RU, United Kingdom piergiorgio.gentile@newcastle.ac.uk

[4] Biomedical Components s.r.l., Via Calopinace Arg. Dx, 6, 89128 Reggio Calabria , Italy

giuseppe.falvodursolabate@enginlife.com

[*] Dr. Chiara Tonda-Turo

Department of Mechanical and Aerospace Engineering

Politecnico di Torino

Corso Duca degli Abruzzi 24, Torino, Italy

telephone number: 0039 0903395

fax number: 0039 0906999

e-mail address: chiara.tondaturo@polito.it

ABSTRACT

Chitosan (CS) membranes obtained by electrospinning are potentially ideal substrates for soft tissue engineering as they combine the excellent biological properties of CS with the extracellular matrix (ECM)-like structure of nanofibrous mats. However, the high amount of acid solvents required to spun CS solutions interferes with the biocompatibility of CS fibres. To overcome this limitation, a novel CS based solutions were investigated in this work. Low amount of acidic acid (0.5 M) was used and dibasic sodium phosphate (DSP) was introduced as ionic crosslinker to improve nanofibres water stability and to neutralize the acidic pH of electrospun membranes after fibres soaking in biological fluids. Randomly oriented and aligned nanofibres (118 ± 16 nm size) were obtained through electrospinning process (voltage of 30 kV, 30 μL/min flow rate and temperature of 39 °C) showing mechanical properties similar to those of soft tissues (Young Modulus lower than 40 MPa in dry condition) and water stability until 7 days. C2C12 myoblast cell line was cultured on CS fibres showing that the aligned architecture of substrate induces cell orientation that can enhance skeletal muscle regeneration.

Keywords: chitosan, ionic crosslinking, electrospinning, skeletal muscle regeneration

List of abbreviations

CS: chitosan

DAPI: 4',6-diamidino-2-phenylindole

DMSO: dimethyl sulfoxide

DSP: dibasic sodium phosphate

ECM: extracellular matrix

EDS: energy dispersive spectrometer

glass-CTRL: glass coverslip

GP: glycerol phosphate

FFT: Fast Fourier Transform

FTIR-ATR : attenuated total reflection Fourier transform infrared

P: phosphorus

PBS: phosphate buffered saline

PCL: poly(caprolactone)

PEO: poly(ethyleneoxide)

PMS: phenazine methosulphate

PVA: poly(vinyl alcohol)

SEM: scanning electron microscopy

TRITC: tetramethylrhodamine

E: Young's modulus

UTS: ultimate tensile strength

$\varepsilon_{failure}$: strain at failure

1. Introduction

Chitosan (CS) is a basic natural polysaccharide obtained by alkaline deacetylation from chitin (Muzzarelli, 2009) having excellent biocompatibility features and antimicrobial activity which foreseen its potential in many medical applications such as drug delivery systems (Bhattarai, Gunn, & Zhang, 2010; J. H. Park, Saravanakumar, Kim, & Kwon, 2010), wound-healing agents (Howling et al., 2001; Murakami et al., 2010) and peripheral nerve repair (Amado et al., 2008; Li et al., 2014). The possibility to process CS into nanofibres has been largely investigated to produce nanofibrous substrate able to mimic the extracellular matrix (ECM) structure (N. Bhattarai, D. Edmondson, O. Veiseh, F. A. Matsen, & M. Zhang, 2005a; Z. G. Chen, Wang, Wei, Mo, & Cui, 2010). A number of fabrication techniques have been explored to prepare micro/nanoscale fibrous scaffolds, among which, electrospinning method has been widely accepted as the simplest and least expensive one to fabricate fibrous matrices through the extrusion of the solution from a needle by an high voltage electric field (Agarwal, Wendorff, & Greiner, 2008; Koh, Yong, Chan, & Ramakrishna, 2008; Tonda-Turo et al., 2013b). Random or aligned fibres can be obtained mimicking the ECM architecture of different tissues (e.g. nerves and tendons have an aligned structure while skin and cartilage have a random structure) as many studies have shown that the fibre orientation influences cell adhesion, growth and modulates elongated cellular patterns that are typical of morphology found in native tissue (Choi, Lee, Christ, Atala, & Yoo, 2008; Corey et al., 2007; Gnavi et al., 2015; Gupta et al., 2009; Neal et al., 2012; Qu et al., 2012; Yang, Murugan, Wang, & Ramakrishna, 2005).

The electrospinnability of CS is limited mainly by its polycationic nature in solution, rigid chemical structure and specific inter and intra-molecular interactions which makes CS solutions highly viscous at low acid pH and room temperature (Homayoni, Ravandi, & Valizadeh, 2009).

However, processing conditions have to be carefully selected as the use of high temperatures and organic solvents may cause CS denaturation and could interfere with CS biocompatibility (Ghasemi-Mobarakeh, Prabhakaran, Morshed, Nasr-Esfahani, & Ramakrishna, 2008). In order to overcome these drawbacks, CS nanofibre fabrication has been attempted using blends with easy spinnable polymers, such as poly(ethyleneoxide) (PEO) (Bhattarai, et al., 2005a; Sarkar, Farrugia, Dargaville, & Dhara, 2013), poly(vinyl alcohol) (PVA) (Charernsriwilaiwat, Opanasopit, Rojanarata, Ngawhirunpat, & Supaphol, 2010; Duan et al., 2006) and poly(caprolactone) (PCL) (Cooper, Bhattarai, & Zhang, 2011), silk fibroin (Z. X. Cai et al., 2010; W. H. Park, Jeong, Yoo, & Hudson, 2004) and collagen (L. Chen et al., 2011; Z. G. Chen, Mo, & Qing, 2007). Although several studies have been reported, the use of CS electrospun nanofibres remains largely unexplored and further experiments are necessary to define process parameter for successful CS nanofibres fabrication. In this work, a novel procedure to electrospun CS nanofibres was developed using low amounts of acetic acid (0.5 M) for CS solubilization in order to reduce the risk of cytotoxic residues and polymer degradation.

A particular focus of the study was the use of dibasic sodium phosphate (DSP) in novel one-step crosslinking of the CS. DSP is negatively charged in aqueous solution enabling it to bind preferentially with dissolved acidic chitosan quaternary ammonium cation providing ionic crosslinking of the CS (Fig. 1). The one-step crosslinking method offer many advantages compared to the two-step method in terms of repeatability and fine tuning of fibres morphology. DSP was selected as CS non-covalent crosslinker for its ability to increase the CS solution pH without causing CS precipitation and/or increased in solution viscosity. Tailoring the amount of DSP, an increase of CS solution pH from 4 to 5.8-5.9 was achieved. This increase in the solution pH was sufficient to maintain physiological pH (around 7) in the CS membrane surrounding

environment after immersion in biological fluids (Ruini, Tonda-Turo, Chiono, & Ciardelli, 2015) without affecting the viscosity of the CS solution and/or interfering with the crosslinking process (Ruini, et al., 2015). Ionic crosslinkers, such as DSP and glycerol phosphate (GP), have been already applied for CS based porous scaffolds and hydrogels (Kim et al., 2010; Ruini, 2015) while, to the best of our knowledge, the ionic crosslinking combined with low amounts of acid solution for nanofibres fabrication was applied in this study for the first time. Kielchel et al. reported the fabrication of GP crosslinked CS nanofibres using a one-step method, however an elecrospinnable solution was obtained with a high amount of trifluoroacetic acid (99%) and fabricated fibres show a ribbon-like morphology with many defects (Kiechel & Schauer, 2013).

In this work, CS crosslinked nanofibres were produced as randomly oriented or as aligned fibres (using high speed drum electrode collection) and characterized by scanning electron microscopy (SEM), infrared spectroscopy (FTIR-ATR), uniaxial tensile mechanical testing, and dissolution studies. An *in vitro* cell assay was included in the study as a preliminary investigation of the applicability of the novel CS membrane as a cellular scaffold in tissue engineering applications. A C2C12 myoblast cell line was used to examine cellular adherence and proliferation on the novel membranes.

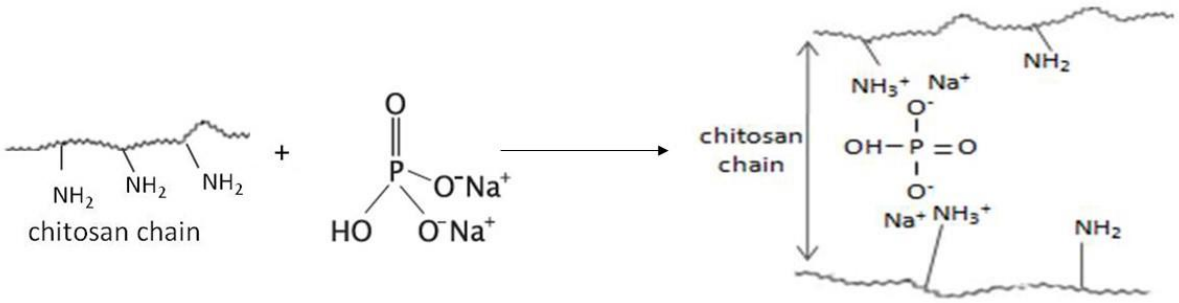

Fig. 1. Scheme of CS crosslinked DSP (non-covalent crosslinker), reproduced with permission from (Ruini, et al., 2015).

2. Materials and methods

2.1 Materials

Medical grade CS (molecular weight 200 – 400 kDa, deacetylation degree ≥ 92.6 %) was purchased from Kraeber GmbH & Co. PEO (M_w 900.000 Da), DSP, dimethyl sulfoxide (DMSO) and solvents were supplied from Sigma Aldrich. All solvents were of analytical grade and were used without further purification.

2.2 Electrospun membrane preparation

2.2.1 Preparation of solutions for electrospinning

Different CS (3, 5 or 7 % (w/v)) and 3% (w/v) PEO solutions were prepared separately by dissolving CS or PEO in 0.5 M acetic acid solution at room temperature by continuous stirring. After complete solubilisation of each components, a 50/50 (v/v) CS/PEO solution was prepared by mixing equal volumes of CS and PEO solutions to obtain the mixtures with weight ratios of CS to PEO of 50/50, 62/38 and 70/30; the resultant mixtures were kept under stirring for about 2 hours. A 5% (v/v) of dimethyl sulfoxide (DMSO) was added to the CS/PEO solution as a co-solvent to relax CS chain entanglements and increase the fibre yields and consequently improving the spinnability of the CS-based solution (N. Bhattarai, D. Edmondson, O. Veiseh, F. A. Matsen, & M. Q. Zhang, 2005b). The pH of this solution was around 4. Finally, ionically crosslinked samples (CS/PEO_DSP) were prepared by adding 1M DSP (one drop per second) to the CS/PEO solution with a concentration of 7.5 % v/v with respect to the natural polymer solution volume. One molar DSP solution was used as it represents its maximum solubility in aqueous solution. The amount of DSP solution added to CS solution was selected to avoid CS precipitation (final clear solution) and to reach a final CS solution pH around 5.8-5.9 which guarantees to maintain

physiological pH of CS-based scaffold after immersion in physiological solution, as previously described by Ruini et al. (Ruini, 2015; Ruini, et al., 2015). Uncrosslinked solutions were prepared as control samples.

2.2.2 Electrospinning of CS nanofibres

The electrospinning system used for fibre preparation was previously described (Tonda-Turo et al., 2013a). Briefly, the electrospinning system was kindly supplied by Biomedical Components s.r.l and it consists of a high voltage generator (PS/EL30R01.5-22 Glassman High Voltage), providing a voltage from 0 to 30 kV; a volumetric pump (KDS210 of KD Scientific); a mobile syringe support and a collector. In this study, two different collectors were used: a 1.5 mm-thick flat aluminium collector for random fibres preparation and a cylindrical rotating drum having a 80 mm diameter and a controllable rotating speed from 0 to 2400 rpm. Before characterization, all CS nanofibres were peeled off from the collector.

2.3 Membrane preparation and optimization of solution and process parameters

2.3.1 Solution parameters and viscosity tests

Preliminary tests were performed to optimize the amount of CS in the CS/PEO_DSP solution. Three CS/PEO_DSP solutions were tested having different CS/PEO ratio: 50/50 (coded as 3% CS), 62/38 (coded as 5% CS) and 70/30 (coded as 7% CS). A stress-controlled rheometer (MCR302, Anton Paar GmbH), equipped with 50 mm parallel plates geometry was used. For temperature control a Peltier system was employed. Samples were put on the lower plate at 40 °C, maintained in quiescent conditions for 15 minutes to reach the thermal stability and finally

175 isothermally tested (40 °C). The viscosity was checked at constant temperature by means of flow
176 curves with shear rate control (shear rate from 1 to 100 s^{-1}).

177 **2.3.2 Process parameters**

178 Continuous nanofibres were obtained only for CS solution concentration of 5 % (62/38 w/w
179 CS/PEO mixture). Process parameters were varied to reduce fibre defects and maximize the
180 amount of collected material. The parameter values allowing spinnability were: (i) temperature
181 from 25 °C to 39 °C, (ii) flow rate of 25 µl min^{-1} to 50 µl min^{-1}, (iii) nozzle-collector distance of
182 12 cm, and (vi) voltage of 30 kV. The effect of temperature and flow rate was evaluated to
183 optimize the process and the fibre morphology.

184

185 **2.3.3 Fibres morphology and element distribution**

186 The surface morphology of uncrosslinked and crosslinked CS based nanofibrous membranes was
187 observed by scanning electron microscopy (SEM LEO – 1430, Zeiss) using an accelerating
188 voltage of 15 kV, a working distance of 10 mm and a Tungsten filament. Qualitative
189 compositional analysis and punctual elemental composition of materials were performed using an
190 energy dispersive spectrometer (EDS) on a 40µm x 40 µm area. Samples were sputter coated with
191 gold in an under-vacuum chamber prior to SEM-EDS examination. In EDS analysis the gold peak
192 was omitted using the INCA software prior to elemental mapping.
193 SEM micrographs were then analysed through Image1.44g software. Fibre diameters and pores
194 were measured on three different SEM micrographs (30 measures were taken for each image) and
195 reported as average value ± standard deviation.
196 Crosslinked nanofibre orientation at different process conditions was examined through 2D Fast
197 Fourier Transform (FFT) ImageJ processing tool. The applied processing tool shows graphical

peaks indicating predominant fibre orientation angles. 2D FFT plots having two sharp peaks at a distance of 180° are typical of oriented structures (Jha et al., 2011; Wu, Fan, Chu, & Wu, 2010).

2.4 Electrospun membranes characterization

2.4.1 Fourier transform infrared-attenuated total reflectance spectroscopy (FTIR-ATR)

Chemical characteristics of the uncrosslinked and crosslinked CS nanofibrous scaffolds were evaluated by an attenuated total reflection Fourier transform infrared (ATR-FTIR) spectrophotometer (Perkin-Elmer). Spectra were obtained in the range of 2000-600 cm^{-1} with a resolution of 4 cm^{-1} and 16 scans. A diamond crystal and an angle of incidence of the contact beam of 45° were used. The spectra are reported after blank subtraction (spectrum without sample).

2.4.2 Mechanical properties

The tensile mechanical properties were evaluated on uncrosslinked and crosslinked nanofibrous membranes in dry condition using a MTS QTest/10 device equipped with load cells of 10 N. Rectangular specimens of 30 mm x 5 mm size were cut from each membranes and their thickness were measured using a digital calibrator. Samples were then strained at a constant crosshead speed of 1 mm/min until breaking; for oriented nanofibres the stress direction was parallel to the fibre alignment. Break stress and strain were determined using the associated software Test Works 4 while the elastic moduli (E) were calculated from the slope of the linear portion of the stress–strain curve of each sample. Five specimens for each kind of material were tested. The results were expressed as average value ± standard deviation.

2.4.3 Fibres dissolution

The dissolution behavior of the uncrosslinked and crosslinked CS samples (randomly oriented and aligned) was evaluated by immerging the samples in phosphate buffered saline (PBS, pH 7.4) at 37°C. After 1, 3, 5 and 7 days immersion, qualitative test was performed analyzing the nanofibres morphology by SEM. Prior to morphological analysis, samples were removed from PBS at each time step and freeze-dried for 24 hours. The solution pH was measured at the same time intervals and three measurements were performed at each time points using a pH meter (XS Instruments).

2.5 *In vitro* characterization using C2C12 myoblast cell line

C2C12 myoblast cell line (ATCC CRL1772), isolated from mouse muscle was used. Cells were cultured in DMEM enriched with 10% fetal bovine serum, glutamine (2mM), penicillin (100 U/ml), and streptomycin (100mg/ml) (Euroclone, Italy). $2*10^4$cells/cm^2 cells were cultured on randomly oriented and aligned crosslinked CS fibres for 3 and 6 days. Tests were performed in triplicate. Cells cultured on glass coverslips (glass-CTRL) were used as control.

Cell viability has been measured using a colorimetric method (CellTiter 96® Aqueous Non-Radioactive Cell Proliferation Assay — Promega, Italy). The CellTiter 96® AQueous Assay is composed of solutions of a novel tetrazolium compound [3-(4,5-dimethylthiazol-2-yl)-5-(3-carboxymethoxyphenyl)-2-(4-sulfophenyl)-2H-tetrazolium, inner salt; MTS] and an electron coupling reagent phenazine methosulphate (PMS). MTS is bioreduced by cells into a formazan product that is soluble in culture medium. The absorbance of the formazan product at 490 nm can be measured directly in 96-well assay plates. The conversion of MTS into the aqueous soluble formazan product is accomplished by dehydrogenase enzymes found in metabolically active cells.

The quantity of formazan product as measured by the amount of 490 nm absorbance is directly proportional to the number of living cells.

Briefly, at each time point cell culture medium was removed and MTS solution was added into each assay-plate; after 4 h incubation of cells with MTS solution, the UV–vis absorbance of the solution at 490 nm was measured.

Cell morphology on different surfaces was observed through fluorescent microscopy (Leica Microsystems DM2500) at 20X and 40X magnifications. At 3 and 6 days, cells were fixed in formaldehyde 4% for 60 min at room temperature. After rinsing, phalloidin - tetramethylrhodamine (TRITC) conjugated (Sigma, Italy) was incubated for 45 min at 37°C in the dark. For nuclear staining and 4',6-diamidino-2-phenylindole (DAPI) was used.

The stability of the nanofibrous mats after cell culture was confirmed using a scanning electron microscope (SEM, LEO – 1430, Zeiss). To perform SEM analysis, the medium was removed and samples were washed twice in 0.15M cacodylate buffer and fixed for 30 minutes at 4°C with Karnowsky solution (2% paraformaldehyde and 2,5% gluteraldehyde in 0.15M cacodylate buffer, pH 7.2-7.4). Following fixation, samples were treated for 30 minutes with 1% osmium tetroxide in 0.15M cacodylate buffer solution. Samples were then dehydrated with graded ethanol (25%, 50%, 75%, 90% and 100%), dried and sputter-coated with gold-palladium prior to SEM analysis.

2.6 Statistical Analysis

Statistical analysis was performed applying t-Student for two group comparisons and one-way ANOVA for multiple analysis using GraphPad Prism 6.0 software. Data were considered statistically different for p value < 0.05.

3. Results and discussion

3.1 Optimization of the electrospinning parameters

3.1.1 Solution viscosity and its effect on electrospun nanofibres

The effect of CS solution concentration on viscosity and, consequently, spinnability was evaluated. The three solutions analysed showed a non-newtonian behavior and an increase in viscosity for more concentrate CS solutions (Fig. 2A). Homogenous nanofibres were obtained only for 5% solution (Fig. 2C), while less viscous solution caused the formation on beads instead of fibres (Fig. 2B) and highly concentrated solution impeded the flow of the solution from the needle (Fig. 2D).

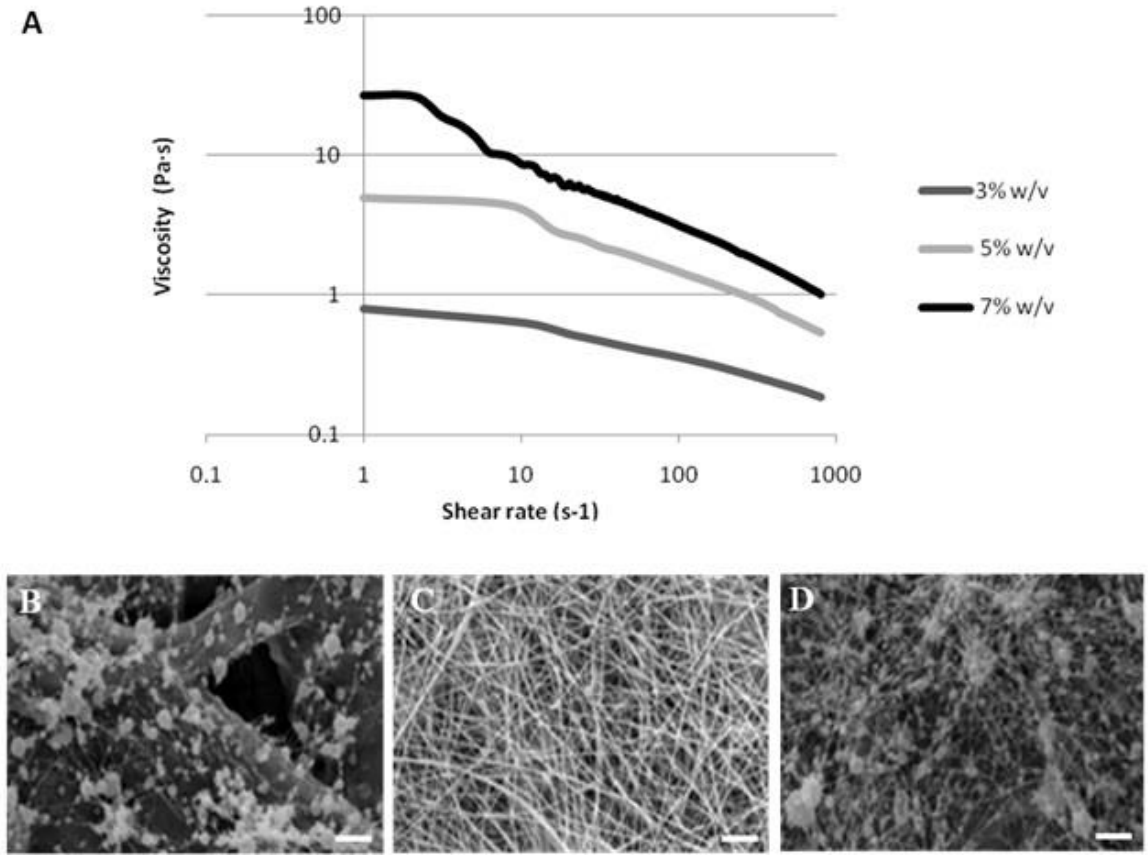

278

279 **Fig. 2.** Viscosity versus shear rate for three different concentration of the CS-based solutions (A).
280 SEM micrographs of electrospun CS mats obtained with a 3% (B), 5% (C) and 7% (D) CS
281 solutions (Parameters: 30kV, temperature 39°C, distance 12 cm, flow rate 30 µL/min). Scale bar:
282 2 µm.

283

284 **3.1.2 Process parameters**

285 The optimization of the process parameters required to vary them in a wild range of sets. For the
286 fabrication on randomly oriented nanofibres, the voltage applied was fixed at 30 kV and the
287 distance between needle and collector was 12 cm. The influence of temperature and flow rate was
288 analyzed to maximize the formation of homogeneous fibres. The 5% solution was spinnable in

289 the range of 25 to 50 μL/min and highly homogenous fibres with a diameters of 118 ± 16 nm were
290 obtained for flow rate of 30 μL/min (Fig. 3). Concerning temperature, an increase in temperature
291 allowed to reduce the number of defects on the fibres as reported in Figure 3. The electrospinning
292 process was set at 39°C.

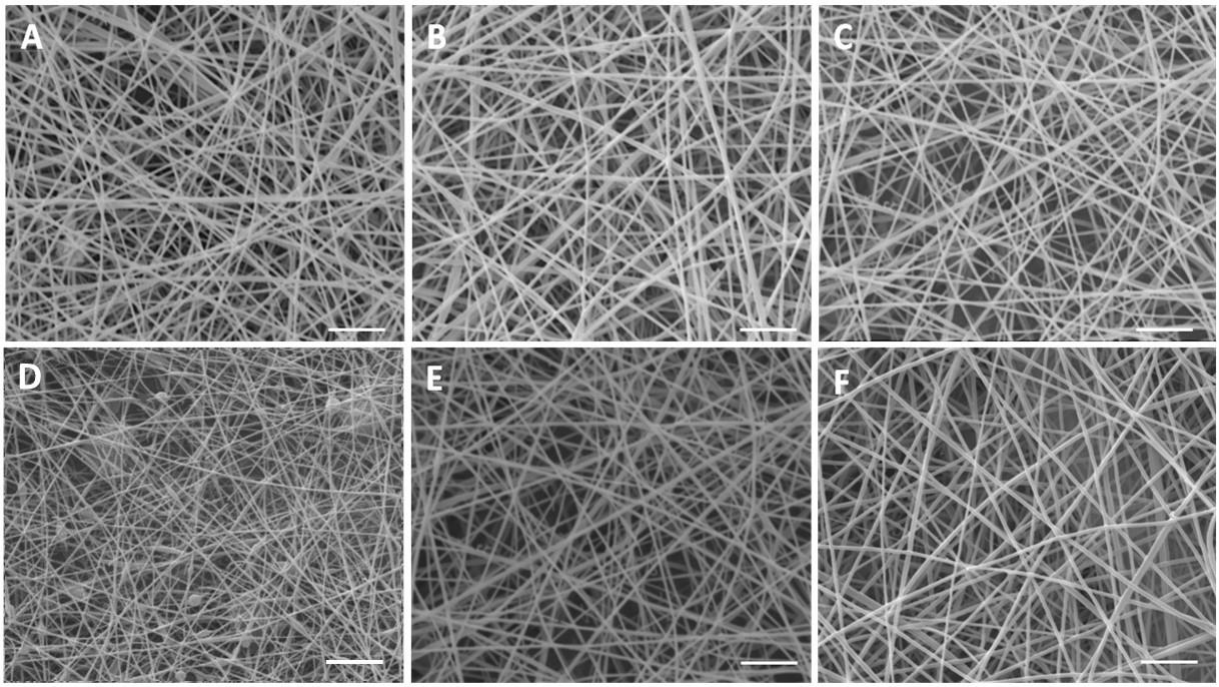

293

294 **Fig. 3.** SEM micrographs of CS randomly oriented nanofibres fabricated at different flow rates
295 (fixed parameters: voltage 30kV, distance nozzle-collector 12 cm, T=39°C): 25 μL/min (A), 27,5
296 μL/min (B), 30 μL/min (C), and at different temperature (fixed parameters: voltage 30kV, distance
297 nozzle-collector 12 cm, flow rate 30 μL/min): 25 °C (D), 32°C (E) and 39 °C (F). Bars: 2 μm.

298

299 The optimized parameters (solution concentration 5%, voltage 30kV, temperature 39°C, distance
300 12 cm, flow rate 30 μL/min) were applied to fabricate aligned CS-based nanofibres. The mandrel
301 rotation was varied from 300 to 2400 rpm to analyze the influence of this parameter on fibre
302 alignment. The FFT analysis of the SEM images was also used to quantitatively analyze the

degree of the CS based nanofibre alignment. A graphical plot of the FFT frequency distribution was generated by summing the pixel intensities encountered along the radius of the FFT output image obtained from the original SEM image. Rotating speed around 300 rpm did not allow fibre orientation as confirmed by SEM image and FTT analysis (Fig. 4A). On the other hand, for rotating speed of 2400 rpm (Fig. 4B), two sharp peaks can be observed at a distance around 180°, confirming that a high amount of fibres is aligned along a preferential direction.

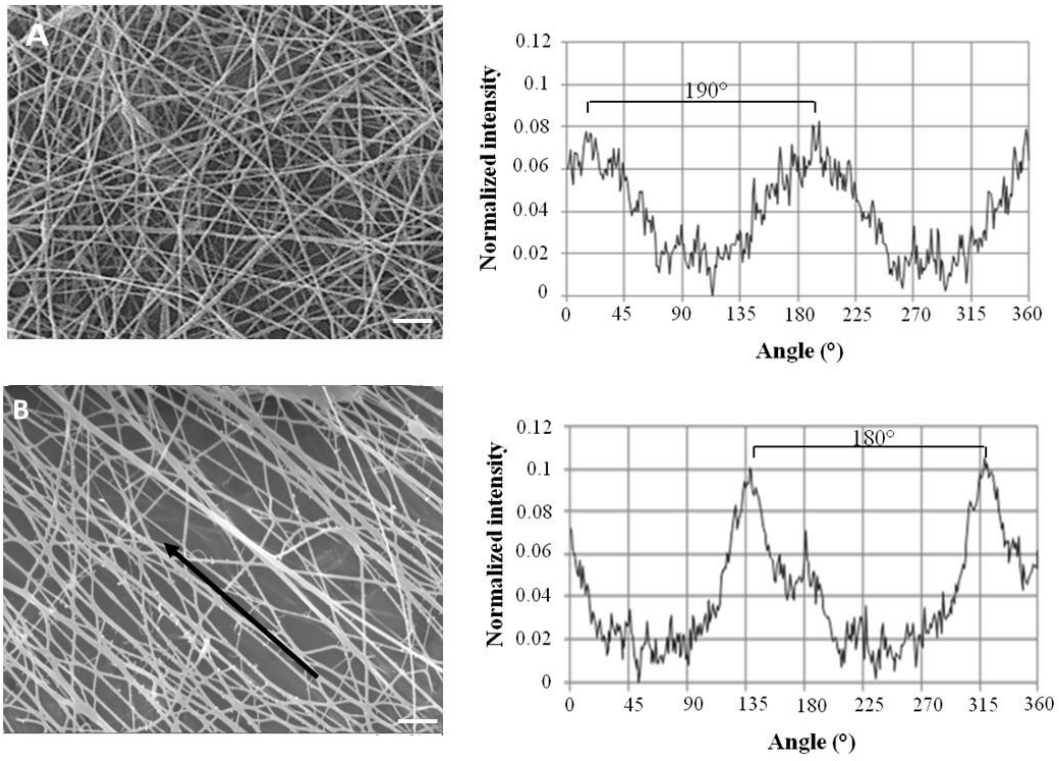

Fig. 4. SEM micrographs and FTT analysis of nanofibres collected using a rotating mandrel rate of 300 rpm (A) and 2400 rpm (B). Arrow indicate the fibre alignment direction. Bars 5 μm.

3.2 Characterization of the CS based nanofibres

3.2.1 Fibres morphology and element distribution

Uncrosslinked and crosslinked fibres obtained using optimized parameters (solution concentration 5%, voltage 30 kV, temperature 39 °C, distance 12 cm, flow rate 30 µL/min) were visualized through SEM and qualitative analysis of phosphorus (P) element was performed using EDS. EDS analysis confirmed the presence of carbon, oxygen and nitrogen, the main elemental components of CS, in all samples (data not shown). Green spots representing phosphorus were found to be homogeneously distributed within both randomly oriented and aligned crosslinked samples confirming the presence of DSP into nanofibers produced using both plane and rotating collectors (Fig. 5B and C). No green spots were detected on uncrosslinked samples (Fig. 5A). The insets in figure 5 display the corresponding morphologies. Highly uniform and smooth nanofibres were formed without the occurrence of bead defects for all the nanofibrous scaffolds. Randomly oriented and aligned nanofibres size was no significantly different with values of 128 ± 19 nm and 140 ± 41 nm, respectively, showing comparable values to uncrosslinked CS nanofibrous samples (109 ± 17 nm). The pore size was in the range of 1-3 µm for both random, aligned, crosslinked and uncrosslinked membranes. Membrane microporosity guarantees a high number of site for cell adhesion.

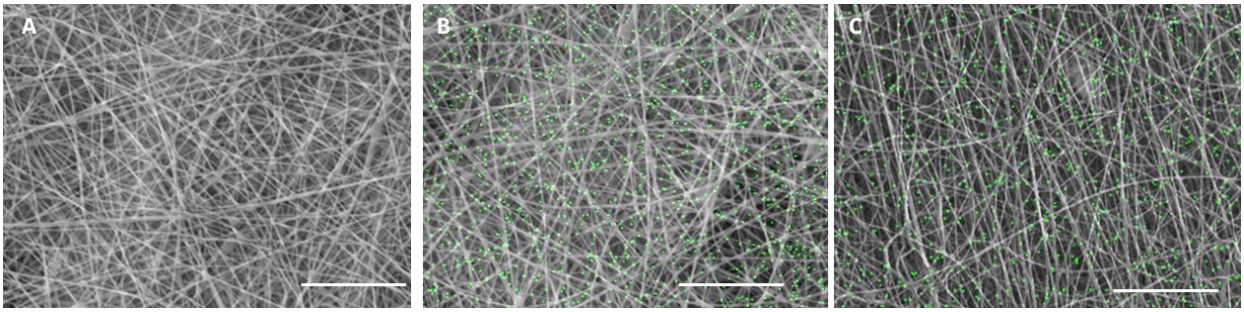

Fig. 5. EDS elemental mapping and SEM images of uncrosslinked (A) and crosslinked randomly oriented (B) and aligned (C) CS-based nanofibres. Green spots correspond to phosphorus (P) elements. Bars 10 μm.

3.2.2 Fourier transform infrared-attenuated total reflectance spectroscopy (FTIR-ATR)

FTIR spectra of uncrosslinked and crosslinked randomly oriented CS-based nanofibres presented the peaks related to CS and PEO, which are present in the CS-based nanofibres (figure 6). Peak wavenumbers and their relative bond vibrations are reported in Table 1. For CS-based nanofibres, the appearance of the peak at 1074 cm^{-1} is related to the stretching of S=O bonds ($\nu_{S=O}$) due to the presence of DMSO residues in the nanofibres, in accordance to results obtained by Markarian et al. (Markarian, Gabrielyan, & Grigoryan, 2004). Furthermore, in the crosslinked nanofibres the crosslinking was confirmed by the appearance of peaks at 1059 cm^{-1}, 944 cm^{-1} and 858 cm^{-1} related to PO_3 stretching (νPO_3), O-P-O bending (δO-P-O) and P-OH bending (νP-OH), respectively (Larkin, 2011). No differences were observed between FTIR-ATR spectra of randomly oriented and aligned nanofibres.

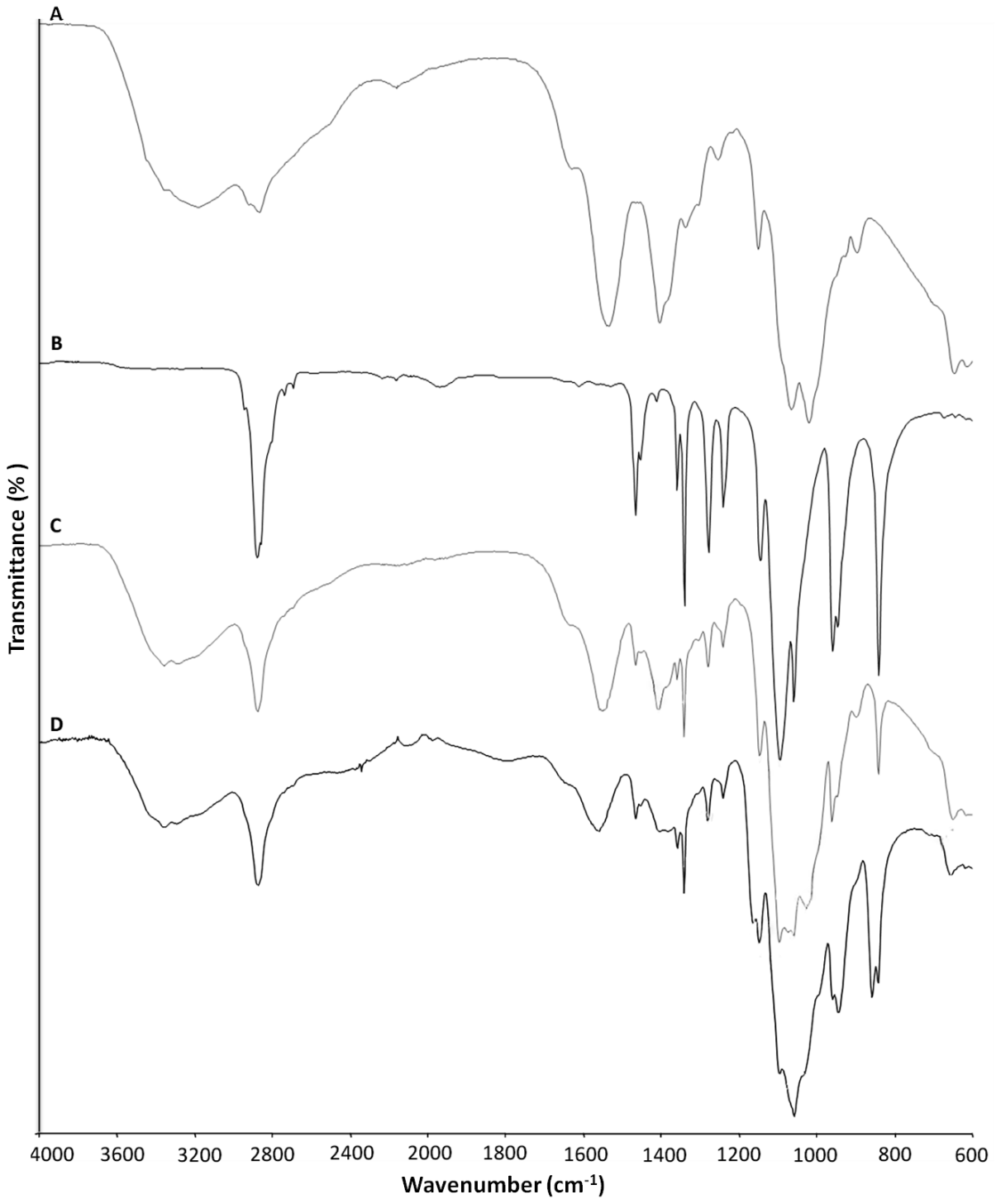

Figure 6. FTIR spectra of CS (A), PEO (B), uncrosslinked CS nanofibers (C), crosslinked CS nanofibers (D).

353 **Table 1.** FTIR peaks and their relative bond vibrations.

Bond vibration	Wavenumber (cm^{-1})	Material	ref
νO-H	3222	CS	(Rubilar et al., 2013)
νN-H			
νC-H	2883	CS and PEO	(Duan, Dong, Yuan, & Yao, 2004; Ojha et al., 2008)
νC=O	1634	CS	(Duan, et al., 2004; Kjm, Son, Kim, Weller, & Hanna, 2006; Rubilar, et al., 2013)
δN-H	1547	CS	(Duan, et al., 2004; Kjm, et al., 2006; Leceta, Guerrero, & de la Caba, 2013; Rubilar, et al., 2013)
δCH_2	1466	PEO	(Dey, Das, Karan, & De, 2011)
νC-N	1410	CS	(Leceta, et al., 2013)
ωCH_2	1360	PEO	(Dey, et al., 2011)
τCH_2	1280; 1241	PEO	(Dey, et al., 2011)
νC-O-C	114; 1095; 1060	CS and PEO	(Caykara, Demirci, Eroglu, & Guven, 2005; Duan, et al., 2004)
ρCH_2	959; 947	PEO	(Dey, et al., 2011)
δC-O-C	842	PEO	(Caykara, et al., 2005)

354

355

3.2.3 Mechanical properties

The mechanical behaviour of uncrosslinked and crosslinked (randomly oriented and aligned) CS fibrous matrices was determined in dry condition. A stress-strain plot for the CS based nanofibres was obtained and the average Young's modulus (tensile elastic modulus), ultimate tensile strength (UTS) and strain at failure ($\varepsilon_{failure}$) were determined. Young's moduli were calculated from the slope of the linear elastic region of the stress-strain curve (Table 2) while UTS and $\varepsilon_{failure}$ were the values at break.

Table 2. Young's modulus (E), ultimate tensile strength (UTS) and strain at failure ($\varepsilon_{failure}$) of the electrospun membranes with random and aligned fibres.

Sample	**E (MPa)**	**UTS (MPa)**	**$\varepsilon_{failure}$ (%)**
Uncrosslinked random	35±7	1.8±0.5	3.5±0.6
Crosslinked random	42 ±12	1.1±0.3	3.2±0.5
Crosslinked aligned	14±6	0.9±0.2	8.1±0.9

Uncrosslinked and crosslinked randomly oriented CS nanofibres showed comparable results to nanofibrous membranes. However, following the alignment of crosslinked nanofibres, the E decreased significantly (*$p < 0.05$). During the fabrication of the aligned structure, the high speed rotation of the mandrel caused a fibres pre-loading which consequently resulted in a reduction of the measured E. Concerning the $\varepsilon_{failure}$ values, an increased in elongation was obtained for aligned samples as a consequence of the ordered structure parallel to the stress direction (Cooper, et al., 2011).

Concerning tissue engineering, biomaterial constructs should ideally resemble the *in vivo* mechanical and structural properties of the tissues that they are intended to replace (Fung 1993 Biomechanics: mechanical properties of living tissues. 2nd ed. New York: Springer).

Based on the mechanical properties of the scaffolds, the electrospun nanofibrous matrices are indicated for soft tissue applications, such as skin, cartilage and nerve (Hung, Chang, Lin, Walter, & Bunegin, 1981; Mow & Guo, 2002).

3.2.4 Fibres dissolution

To confirm the effectiveness of the crosslinking process and to evaluate the stability of CS based nanofibres in aqueous environment, a qualitative analysis of the dissolution behaviour of uncrosslinked and crosslinked CS based nanofibres was performed in PBS at 37°C. The soaking solution pH was monitored and values of 7.2 ± 0.2 were detected at each time point. Figure 7 illustrates the morphological changes in nanofibres during *in vitro* dissolution. All nanofibrous matrices showed swelling during the first hour after immersion in aqueous solutions, though significant morphological changes were not observed. After 7 days incubation in PBS, partial dissolution of the fibres was observed for uncrosslinked nanofibres. On the other hand, both crosslinked aligned and randomly oriented nanofibres showed a stable morphology at 7 days confirming the effect of the crosslinker on nanofibres water stability. Furthermore, the aligned structure of CS based nanofibres was maintained after one week of immersion in PBS.

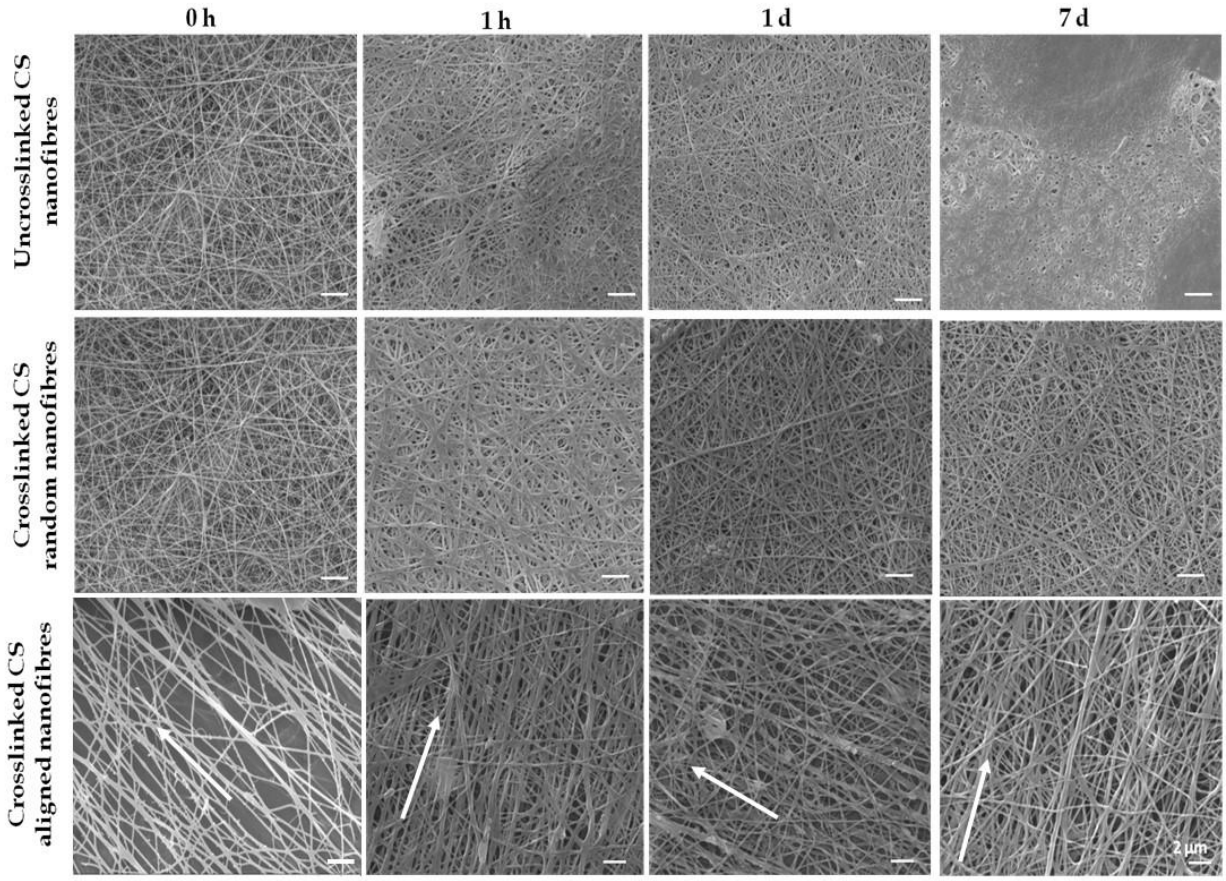

392

393 **Fig. 7**. SEM images of uncrosslinked and crosslinked nanofibres before immersion in PBS (0 h)
394 and after 1 hour (1 h), 1 day (1 d) and 7 days (7 d) dissolution in PBS. Arrows indicate the fibre
395 alignment direction.

396

397 **3.3 *In vitro* characterization using C2C12 myoblast cells: cell viability and morphology**

398 Cell viability in contact with nanofibrous membranes was evaluated with MTS assay, using direct
399 contact tests (cells cultured on biomaterials) and indirect tests (cells cultured with eluates obtained
400 from media maintained for 24 hours at 37°C together with tested materials). Indirect tests did not
401 show any toxic effect due to the present of leached products confirming the biocompatibility of

CS nanofibers (Fig. 8A). During direct contact tests, random and aligned biomaterials were less performing as compared to control (Fig. 8B). After 3 days, the number of cells adhered to the CS fibres is significantly lower compared to cells on control surfaces. However, the number of cells increased with increasing incubation time on both CS nanofibres and control. Therefore, the CS nanofibres developed were biocompatible substrates for the attachment and proliferation of C2C12, even though significantly higher adhesion of C2C12 were observed within the first 3 days on glass coverslips compared to the CS nanofibres. Low cells adhesion followed by cell growth in the next days has been reported on for CS based flat films (Fregnan et al., 2016), porous sponges (Seol et al., 2004) and nanofibres (Kang et al., 2010). The ability of natural polymers to adsorb water, and consequently swell after immersion into physiological media, causes a softening of the material (Ruini, et al., 2015) that could be related to the reduction in initial cell adhesion compered to rigid glass or polypropylene cell culture plates.

Cells cultured on aligned fibres showed a good viability and significantly increase up to 6 days without showing substantial differences with respect to proliferation trend of control. Random fibres resulted as non-ideal substrates for myoblast proliferation as fluorescence analysis showed well spread cells growing as cellular cluster. Cells seeded on aligned fibres showed an adequate spread morphology as well and cell oriented with fibres. The analysis of cell morphology on the investigated substrates revealed that C2C12 cultured onto nanofibres displayed markedly different cell morphologies, with respect to cells cultured onto aligned fibres as shown by phallodin staining (Fig. 8C). After 3 and 6 days, cells cultured on nanofibres mainly presented elongated aspect. Furthermore, aligned biomaterials led to cell alignment on a preferential direction reproducing the ordered structure on muscular tissue. The same morphology was maintained up to 6 days and cell proliferation was observed. The effect of aligned structures on cell morphology and, consequently,

the possibility to instruct cells *in-vitro* to organize their morphology in a specific structure is a promising tool to recreate physiological-like biological tissue.

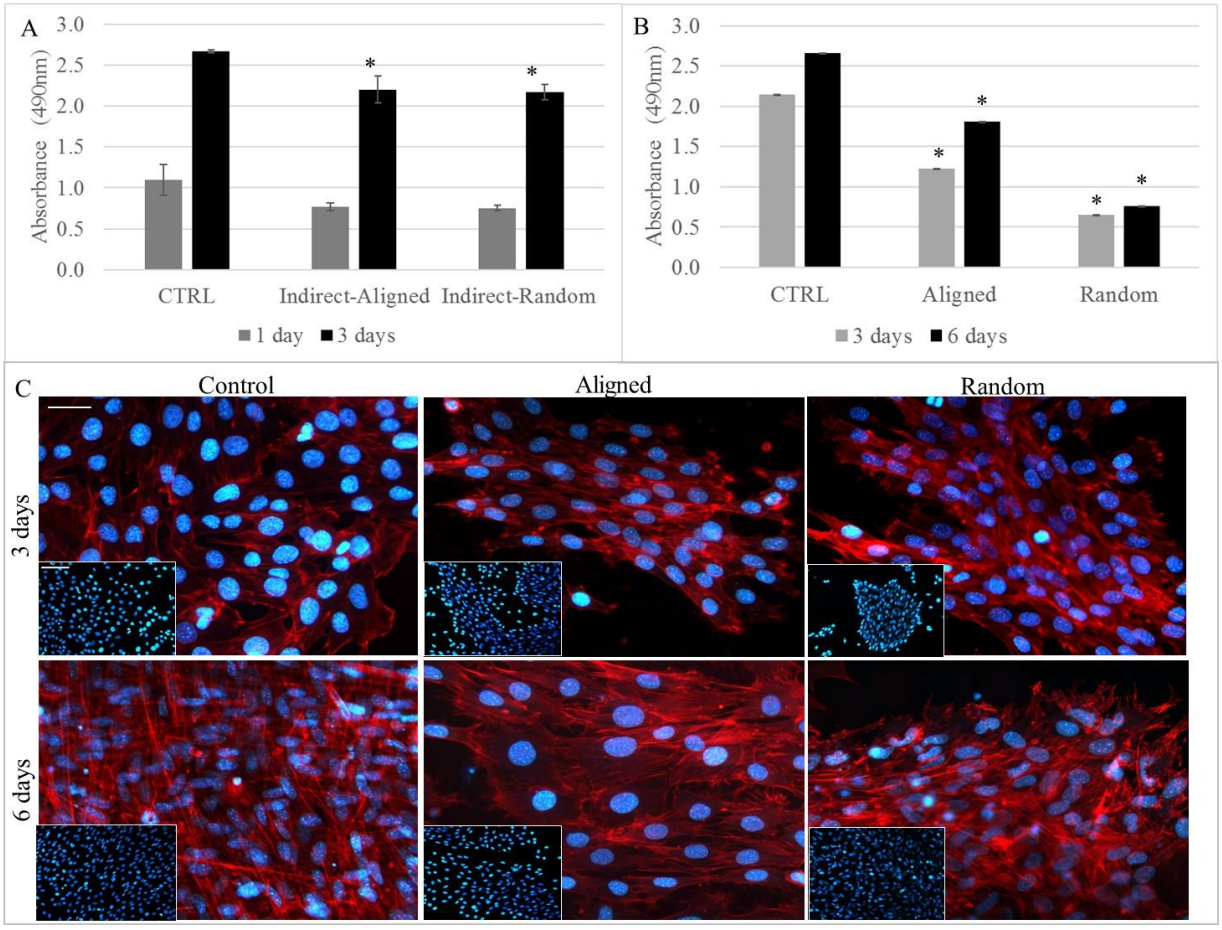

Fig. 8. MTS assay on C2C12: indirect test (A) and direct test (B). Fluorescent microscopy images after TRITC - phalloidin (actin filaments) and DAPI (nuclei) staining after 3 and 6 days of culture (B). Figures are representative of three different experiments. Random and aligned refer to cells cultured directly on CS based nanofibres. Cover glass is used as control. * indicates statistical significance with respect to control with $p \leq 0.01$. Bars: 10 µm and 20 µm (insert).

Finally, SEM images show a stable nanofibrous structure within cell culture time points. The presence of non-degraded nanofibres after cell tests confirmed the ability of DSP crosslinking to enhance CS fibres water stability increasing the fibres dissolution time (Fig.S1).

4. Conclusion

Development of functional tissue engineering products requires an appropriate scaffolding for the treatment of injury and disease to mimic the structure and the biological cues of the native ECM. In this study, electrospun CS based nanofibres were prepared in the form of non-woven and aligned nanofibrous matrices with high specific surface areas and relatively small fibre diameters. Compared to previous work in literature (Ghasemi-Mobarakeh, et al., 2008; Homayoni, et al., 2009) (Kiechel & Schauer, 2013), CS was solubilized in slightly acid solution and without the use of potentially cytotoxic organic solvents. Optimized electrospinning parameters, such as solution concentration, CS/PEO ratio, electric field and temperature allowed to obtained homogenous nanofibres without defects. Finally, an innovative ionic crosslinker (DSP) was used to improve the stability of CS electrospun nanofibres in aqueous environment and to neutralize the residual acid present into the CS nanofibres. A one-step DSP crosslinking method was applied to fabricate crosslinked nanofibrous mats without subsequent post-processing steps (as required in the two-step crosslinking method) that could affect the nanofibrous mats morphology (Kiechel & Schauer, 2013). The crosslinked nanofibres were deposited as a nonwoven membrane or as a highly aligned bundle mimicking the morphology of different tissue characterized by non-oriented or oriented ECM fibrils. Both uncrosslinked and crosslinked CS-based nanofibres were produced showing fibre diameters in a hundred nanometre range which has been reported to be advantageous for chondrocyte (Bhattarai, et al., 2005a; Subramanian, Vu, Larsen, & Lin, 2005), human keratinocyte and fibroblast (Noh et al., 2006) as well as for glial cell adhesion and proliferation (Bhattarai, et al., 2005b; Christopherson, Song, & Mao, 2009). Furthermore, the developed nanofibres showed mechanical properties similar to those of several biological soft tissues such as skin, nerve, muscle. After 7 days in physiological solution, developed nanofibrous mats still

show fibrous morphology. Furthermore, the pH values of soaking solution were maintained into physiological range (7-7.4) thanks to the presence of DSP.

The biocompatible composition of the developed nanofibrous membranes and their biomimetic structure and mechanical properties were assessed through *in vitro* tests using C2C12 myoblast cell line. Our results demonstrated that the topographical constraint generated by the aligned fibres induced the alignment and elongation of C2C12 by contact guidance, also enabling an adequate proliferation on the surfaces. This cell behaviour is important for skeletal muscle regeneration as a pre-requisite for myotubes formation. The CS based membranes are promising surface for muscular cells proliferation and organization into physiological-like structure. Electrospun membranes lack high spacial interconnectivity as only small pores (1-3 μm) can be obtained. To fabricate a macroporous nanofibrous-based scaffold further post-spinning process are required as recently proposed by Cai et al. (Y. Z. Cai et al., 2012). Further work will be addressed to the application of these membranes in the fabrication of 3D macroporous structures to produce scaffold for soft tissue regeneration.

Acknowledgements

Dr P. Gentile, is member of the UK EPSRC Centre for Innovative Manufacturing of Medical Devices. Susanna Sartori is acknowledged for SEM analysis.

References

Agarwal, S., Wendorff, J. H., & Greiner, A. (2008). Use of electrospinning technique for biomedical applications. *Polymer, 49*(26), 5603-5621. doi: DOI 10.1016/j.polymer.2008.09.014

Amado, S., Simoes, M. J., da Silva, P. A. S. A., Luis, A. L., Shirosaki, Y., Lopes, M. A., . . . Geuna, S. (2008). Use of hybrid chitosan membranes and N1E-115 cells for promoting nerve regeneration in an axonotmesis rat model. *Biomaterials, 29*(33), 4409-4419. doi: DOI 10.1016/j.biomaterials.2008.07.043

Bhattarai, N., Edmondson, D., Veiseh, O., Matsen, F. A., & Zhang, M. (2005a). Electrospun chitosan-based nanofibers and their cellular compatibility. *Biomaterials, 26*(31), 6176-6184. doi: S0142-9612(05)00262-0 [pii]
10.1016/j.biomaterials.2005.03.027

Bhattarai, N., Edmondson, D., Veiseh, O., Matsen, F. A., & Zhang, M. Q. (2005b). Electrospun chitosan-based nanofibers and their cellular compatibility. *Biomaterials, 26*(31), 6176-6184. doi: 10.1016/j.biomaterials.2005.03.027

Bhattarai, N., Gunn, J., & Zhang, M. Q. (2010). Chitosan-based hydrogels for controlled, localized drug delivery. *Advanced Drug Delivery Reviews, 62*(1), 83-99. doi: DOI 10.1016/j.addr.2009.07.019

Cai, Y. Z., Zhang, G. R., Wang, L. L., Jiang, Y. Z., Ouyang, H. W., & Zou, X. H. (2012). Novel biodegradable three-dimensional macroporous scaffold using aligned electrospun nanofibrous yarns for bone tissue engineering. *Journal of Biomedical Materials Research Part A, 100A*(5), 1187-1194. doi: 10.1002/jbm.a.34063

Cai, Z. X., Mo, X. M., Zhang, K. H., Fan, L. P., Yin, A. L., He, C. L., & Wang, H. S. (2010). Fabrication of Chitosan/Silk Fibroin Composite Nanofibers for Wound-dressing Applications. *International Journal of Molecular Sciences, 11*(9), 3529-3539. doi: Doi 10.3390/Ijms11093529

Caykara, T., Demirci, S., Eroglu, M. S., & Guven, O. (2005). Poly(ethylene oxide) and its blends with sodium alginate. *Polymer, 46*(24), 10750-10757. doi: DOI 10.1016/j.polymer.2005.09.041

Charernsriwilaiwat, N., Opanasopit, P., Rojanarata, T., Ngawhirunpat, T., & Supaphol, P. (2010). Preparation and characterization of chitosan-hydroxybenzotriazole/polyvinyl alcohol blend nanofibers by the electrospinning technique. *Carbohydrate Polymers, 81*(3), 675-680. doi: DOI 10.1016/j.carbpol.2010.03.031

Chen, L., Zhu, C., Fan, D., Liu, B., Ma, X., Duan, Z., & Zhou, Y. (2011). A human-like collagen/chitosan electrospun nanofibrous scaffold from aqueous solution: electrospun mechanism and biocompatibility. [Research Support, Non-U.S. Gov't]. *Journal of Biomedical Materials Research Part A, 99*(3), 395-409. doi: 10.1002/jbm.a.33202

Chen, Z. G., Mo, X. M., & Qing, F. L. (2007). Electrospinning of collagen-chitosan complex. *Materials Letters, 61*(16), 3490-3494. doi: DOI 10.1016/j.matlet.2006.11.104

Chen, Z. G., Wang, P. W., Wei, B., Mo, X. M., & Cui, F. Z. (2010). Electrospun collagen-chitosan nanofiber: a biomimetic extracellular matrix for endothelial cell and smooth muscle cell. [Research Support, Non-U.S. Gov't]. *Acta Biomaterialia, 6*(2), 372-382. doi: 10.1016/j.actbio.2009.07.024

Choi, J. S., Lee, S. J., Christ, G. J., Atala, A., & Yoo, J. J. (2008). The influence of electrospun aligned poly(epsilon-caprolactone)/collagen nanofiber meshes on the formation of self-

aligned skeletal muscle myotubes. *Biomaterials, 29*(19), 2899-2906. doi: DOI 10.1016/j.biomaterials.2008.03.031

Christopherson, G. T., Song, H., & Mao, H. Q. (2009). The influence of fiber diameter of electrospun substrates on neural stem cell differentiation and proliferation. [Research Support, U.S. Gov't, Non-P.H.S.]. *Biomaterials, 30*(4), 556-564. doi: 10.1016/j.biomaterials.2008.10.004

Cooper, A., Bhattarai, N., & Zhang, M. (2011). Fabrication and cellular compatibility of aligned chitosan–PCL fibers for nerve tissue regeneration. *Carbohydrate Polymers, 85*(1), 149–156.

Corey, J. M., Lin, D. Y., Mycek, K. B., Chen, Q., Samuel, S., Feldman, E. L., & Martin, D. C. (2007). Aligned electrospun nanofibers specify the direction of dorsal root ganglia neurite growth. *Journal of Biomedical Materials Research Part A, 83A*(3), 636-645. doi: Doi 10.1002/Jbm.A.31285

Dey, A., Das, K., Karan, S., & De, S. K. (2011). Vibrational spectroscopy and ionic conductivity of polyethylene oxide-NaClO4-CuO nanocomposite. *Spectrochimica Acta Part a-Molecular and Biomolecular Spectroscopy, 83*(1), 384-391. doi: DOI 10.1016/j.saa.2011.08.050

Duan, B., Dong, C. H., Yuan, X. Y., & Yao, K. D. (2004). Electrospinning of chitosan solutions in acetic acid with poly(ethylene oxide). *Journal of Biomaterials Science-Polymer Edition, 15*(6), 797-811. doi: Doi 10.1163/156856204774196171

Duan, B., Yuan, X. Y., Zhu, Y., Zhang, Y. Y., Li, X. L., Zhang, Y., & Yao, K. D. (2006). A nanofibrous composite membrane of PLGA-chitosan/PVA prepared by electrospinning. *European Polymer Journal, 42*(9), 2013-2022. doi: DOI 10.1016/j.eurpolymj.2006.04.021

Fregnan, F., Ciglieri, E., Tos, P., Crosio, A., Ciardelli, G., Ruini, F., . . . Raimondo, S. (2016). Chitosan crosslinked flat scaffolds for peripheral nerve regeneration. *Biomedical Materials, 11*(4). doi: Artn 045010
10.1088/1748-6041/11/4/045010

Ghasemi-Mobarakeh, L., Prabhakaran, M. P., Morshed, M., Nasr-Esfahani, M. H., & Ramakrishna, S. (2008). Electrospun poly(epsilon-caprolactone)/gelatin nanofibrous scaffolds for nerve tissue engineering. *Biomaterials, 29*(34), 4532-4539. doi: DOI 10.1016/j.biomaterials.2008.08.007

Gnavi, S., Fornasari, B. E., Tonda-Turo, C., Laurano, R., Zanetti, M., Ciardelli, G., & Geuna, S. (2015). The Effect of Electrospun Gelatin Fibers Alignment on Schwann Cell and Axon Behavior and Organization in the Perspective of Artificial Nerve Design. *International Journal of Molecular Sciences, 16*(6), 12925-12942. doi: 10.3390/ijms160612925

Gupta, D., Venugopal, J., Prabhakaran, M. P., Dev, V. R. G., Low, S., Choon, A. T., & Ramakrishna, S. (2009). Aligned and random nanofibrous substrate for the in vitro culture of Schwann cells for neural tissue engineering. *Acta Biomaterialia, 5*(7), 2560-2569. doi: DOI 10.1016/j.actbio.2009.01.039

Homayoni, H., Ravandi, S. A. H., & Valizadeh, M. (2009). Electrospinning of chitosan nanofibers: Processing optimization. *Carbohydrate Polymers, 77*(3), 656-661. doi: DOI 10.1016/j.carbpol.2009.02.008

Howling, G. I., Dettmar, P. W., Goddard, P. A., Hampson, F. C., Dornish, M., & Wood, E. J. (2001). The effect of chitin and chitosan on the proliferation of human skin fibroblasts and

keratinocytes in vitro. *Biomaterials, 22*(22), 2959-2966. doi: Doi 10.1016/S0142-9612(01)00042-4

Hung, T. K., Chang, G. L., Lin, H. S., Walter, F. R., & Bunegin, L. (1981). Stress-Strain Relationship of the Spinal-Cord of Anesthetized Cats. *J Biomech, 14*(4), 269-276. doi: Doi 10.1016/0021-9290(81)90072-5

Jha, B. S., Colello, R. J., Bowman, J. R., Sell, S. A., Lee, K. D., Bigbee, J. W., . . . Simpson, D. G. (2011). Two pole air gap electrospinning: Fabrication of highly aligned, three-dimensional scaffolds for nerve reconstruction. *Acta Biomaterialia, 7*(1), 203-215. doi: DOI 10.1016/j.actbio.2010.08.004

Kang, Y. M., Lee, B. N., Ko, J. H., Kim, G. H., Kang, K. N., Kim, D. Y., . . . Kim, M. S. (2010). In Vivo Biocompatibility Study of Electrospun Chitosan Microfiber for Tissue Engineering. *International Journal of Molecular Sciences, 11*(10), 4140-4148. doi: 10.3390/ijms11104140

Kiechel, M. A., & Schauer, C. L. (2013). Non-covalent crosslinkers for electrospun chitosan fibers. *Carbohydrate Polymers, 95*(1), 123-133. doi: 10.1016/j.carbpol.2013.02.034

Kim, S., Nishimoto, S. K., Bumgardner, J. D., Haggard, W. O., Gaber, M. W., & Yang, Y. Z. (2010). A chitosan/beta-glycerophosphate thermo-sensitive gel for the delivery of ellagic acid for the treatment of brain cancer. *Biomaterials, 31*(14), 4157-4166. doi: 10.1016/j.biomaterials.2010.01.139

Kjm, K. M., Son, J. H., Kim, S. K., Weller, C. L., & Hanna, M. A. (2006). Properties of chitosan films as a function of pH and solvent type. *Journal of Food Science, 71*(3), E119-E124.

Koh, H. S., Yong, T., Chan, C. K., & Ramakrishna, S. (2008). Enhancement of neurite outgrowth using nano-structured scaffolds coupled with laminin. *Biomaterials, 29*(26), 3574-3582. doi: DOI 10.1016/j.biomaterials.2008.05.014

Larkin, P. (2011). *Infrared and Raman Spectroscopy; Principles and Spectral Interpretation* (1st ed.): Elsevier.

Leceta, I., Guerrero, P., & de la Caba, K. (2013). Functional properties of chitosan-based films. *Carbohydrate Polymers, 93*(1), 339-346. doi: DOI 10.1016/j.carbpol.2012.04.031

Li, G. C., Zhang, L. Z., Wang, C. P., Zhao, X. Y., Zhu, C. L., Zheng, Y. H., . . . Yang, Y. M. (2014). Effect of silanization on chitosan porous scaffolds for peripheral nerve regeneration. *Carbohydrate Polymers, 101*, 718-726. doi: DOI 10.1016/j.carbpol.2013.09.064

Markarian, S. A., Gabrielyan, L. S., & Grigoryan, K. R. (2004). FT IR ATR study of molecular interactions in the urea/dimethyl sulfoxide and urea/diethyl sulfoxide binary systems. *Journal of Solution Chemistry, 33*(8), 1005-1015. doi: Doi 10.1023/B:Josl.0000048050.47474.Fc

Mow, V., & Guo, X. E. (2002). Mechano-electrochemical properties of articular cartilage: Their inhomogeneities and anisotropies. *Annual Review of Biomedical Engineering, 4*, 175-209. doi: 10.1146/annurev.bioeng.4.110701.120309

Murakami, K., Aoki, H., Nakamura, S., Nakamura, S., Takikawa, M., Hanzawa, M., . . . Ishihara, M. (2010). Hydrogel blends of chitin/chitosan, fucoidan and alginate as healing-impaired wound dressings. *Biomaterials, 31*(1), 83-90. doi: DOI 10.1016/j.biomaterials.2009.09.031

Muzzarelli, R. A. A. (2009). Chitins and chitosans for the repair of wounded skin, nerve, cartilage and bone. *Carbohydrate Polymers, 76*(2), 167-182. doi: DOI 10.1016/j.carbpol.2008.11.002

Neal, R. A., Tholpady, S. S., Foley, P. L., Swami, N., Ogle, R. C., & Botchwey, E. A. (2012). Alignment and composition of laminin-polycaprolactone nanofiber blends enhance peripheral nerve regeneration. *Journal of Biomedical Materials Research Part A, 100A*(2), 406-423. doi: Doi 10.1002/Jbm.A.33204

Noh, H. K., Lee, S. W., Kim, J. M., Oh, J. E., Kim, K. H., Chung, C. P., . . . Min, B. M. (2006). Electrospinning of chitin nanofibers: Degradation behavior and cellular response to normal human keratinocytes and fibroblasts. *Biomaterials, 27*(21), 3934-3944. doi: 10.1016/j.biomaterials.2006.03.016

Ojha, S. S., Stevens, D. R., Hoffman, T. J., Stano, K., Klossner, R., Scott, M. C., . . . Gorga, R. E. (2008). Fabrication and characterization of electrospun chitosan nanofibers formed via templating with polyethylene oxide. *Biomacromolecules, 9*(9), 2523-2529. doi: Doi 10.1021/Bm800551q

Park, J. H., Saravanakumar, G., Kim, K., & Kwon, I. C. (2010). Targeted delivery of low molecular drugs using chitosan and its derivatives. *Advanced Drug Delivery Reviews, 62*(1), 28-41. doi: DOI 10.1016/j.addr.2009.10.003

Park, W. H., Jeong, L., Yoo, D. I., & Hudson, S. (2004). Effect of chitosan on morphology and conformation of electrospun silk fibroin nanofibers. *Polymer (Guildf), 45*(21), 7151-7157. doi: DOI 10.1016/j.polymer.2004.08.045

Qu, J., Zhou, D. D., Xu, X. J., Zhang, F., He, L. H., Ye, R., . . . Zhang, H. X. (2012). Optimization of electrospun TSF nanofiber alignment and diameter to promote growth and migration of mesenchymal stem cells. *Applied Surface Science, 261*, 320-326. doi: DOI 10.1016/j.apsusc.2012.08.008

Rubilar, J. F., Cruz, R. M. S., Silva, H. D., Vicente, A. A., Khmelinskii, I., & Vieira, M. C. (2013). Physico-mechanical properties of chitosan films with carvacrol and grape seed extract. *Journal of Food Engineering, 115*(4), 466-474. doi: DOI 10.1016/j.jfoodeng.2012.07.009

Ruini, F. (2015). *Chitosan based biomaterials: soft tissue engineering applications.* Doctoral Thesis, Politecnico di Torino, Turin.

Ruini, F., Tonda-Turo, C., Chiono, V., & Ciardelli, G. (2015). Chitosan membranes for tissue engineering: comparison of different crosslinkers. *Biomedical Materials, 10*. doi: 10.1088/1748-6041/10/6/065002

Sarkar, S. D., Farrugia, B. L., Dargaville, T. R., & Dhara, S. (2013). Physico-chemical/biological properties of tripolyphosphate cross-linked chitosan based nanofibers. *Materials Science & Engineering C-Materials for Biological Applications, 33*(3), 1446-1454. doi: DOI 10.1016/j.msec.2012.12.066

Seol, Y. J., Lee, J. Y., Park, Y. J., Lee, Y. M., Young-Ku, Rhyu, I. C., . . . Chung, C. P. (2004). Chitosan sponges as tissue engineering scaffolds for bone formation. *Biotechnology Letters, 26*(13), 1037-1041. doi: Doi 10.1023/B:Bile.0000032962.79531.Fd

Subramanian, A., Vu, D., Larsen, G. F., & Lin, H. Y. (2005). Preparation and evaluation of the electrospun chitosan/PEO fibers for potential applications in cartilage tissue engineering. *Journal of Biomaterials Science-Polymer Edition, 16*(7), 861-873. doi: Doi 10.1163/1568562054255682

Tonda-Turo, C., Cipriani, E., Gnavi, S., Chiono, V., Mattu, C., Gentile, P., . . . Ciardelli, G. (2013a). Cross linked gelatin nanofibres: Preparation, characterisation and in vitro studies using glial-like cells. *Materials Science & Engineering C-Materials for Biological Applications, 33*(5), 2723-2735. doi: 10.1016/j.msec.2013.02.039

Tonda-Turo, C., Cipriani, E., Gnavi, S., Chiono, V., Mattu, C., Gentile, P., . . . Ciardelli, G. (2013b). Crosslinked gelatin nanofibres: preparation, characterisation and in vitro studies using glial-like cells. [Research Support, Non-U.S. Gov't]. *Mater Sci Eng C Mater Biol Appl, 33*(5), 2723-2735. doi: 10.1016/j.msec.2013.02.039

Wu, H. J., Fan, J. T., Chu, C. C., & Wu, J. (2010). Electrospinning of small diameter 3-D nanofibrous tubular scaffolds with controllable nanofiber orientations for vascular grafts. *Journal of Materials Science-Materials in Medicine, 21*(12), 3207-3215. doi: DOI 10.1007/s10856-010-4164-8

Yang, F., Murugan, R., Wang, S., & Ramakrishna, S. (2005). Electrospinning of nano/micro scale poly(L-lactic acid) aligned fibers and their potential in neural tissue engineering. *Biomaterials, 26*(15), 2603-2610. doi: DOI 10.1016/j.biomaterials.2004.06.051